Supplementary information

Beavers can convert stream corridors to persistent carbon sinks

This supplementary information comprises:

Supplementary Text: Texts S1 – S8
Supplementary Figures: Figs. S1 – S8
Supplementary Tables: Tables S1 – S5
References

Supplementary Texts

Text S1: Flow attenuation and subsurface water losses

Substantial discharge attenuation occurred across the reach from January 2022 to January 2023. Median upstream discharge (Q_{US}: 0.12 ± 0.11 $m^3 s^{-1}$) exceeded downstream discharge (Q_{DS}: 0.08 ± 0.08 $m^3 s^{-1}$), with reductions in both baseflow and peak flow (max Q_{US}: 3.42 $m^3 s^{-1}$; max Q_{DS}: 2.35 $m^3 s^{-1}$). The mean net water loss across the reach was 0.05 ± 0.05 $m^3 s^{-1}$, equivalent to 35 ± 23% of upstream inflow.

Solving for Q_s as the residual term in the water balance, subsurface losses are the dominant water loss pathway. It is possible to estimate from this an effective average infiltration rate for the entire wetland area (3.6 ha) of 0.13 ± 0.08 m day^{-1}. Whilst this estimate is informative as a lumped term, it is important to emphasise that, as with many dynamic wetland systems, the actual water losses are likely distributed across a wider range of hydrological pathways, including saturated and unsaturated zones, and also extend as halos beyond the visible inundation boundary, particularly during high-flow events that activate lateral seepage, storage, and even subsequently as evapotranspiration sources for the surrounding forest. This interpretation is supported by the observed seasonal pattern, where subsurface losses peaked in autumn, coinciding with low surface water extents and increasing upstream discharge, conditions consistent with enhanced seepage under drying and draining conditions (Fig. 1b–c). Although we find that wetland evapotranspiration accounts for less than 1% of total water loss at the reach scale, it does significantly contribute to the seasonal dynamics of wetland volume, accounting for ~10 – 20% of volume losses during summer.

Text S2: Aquatic vegetation and deadwood biomass carbon analysis

To quantify the spatial distribution and biomass of aquatic vegetation species, multispectral drone images were collected across the wetland area in January, March, May, August and December 2022. To separate green biomass from water, deadwood, and bare sediment and soil, multispectral information was processed into hyperspectral vegetation and water indices. The spatial cover for each present aquatic species (n = 6; Supplementary Table 2) was analysed using supervised classification with the ArcGIS Pro (3.3.1) toolboxes *Train Support Vector Machine Classifier* and *Classify Raster*, by manually designating known locations of species to specific vegetation index values. Areal biomass density for each species was determined in August 2022 by harvesting material from square plots

(0.16 m^2) in locations with abundant cover of the sampled species. Dry weight of biomass was weighed after oven-drying (80 °C, 48 h). Annual C input from aquatic vegetation was calculated from literature values of C content in dry weight biomass, biomass per area, and the areal cover, for each species respectively (Supplementary Table 2). The daily distribution of C biomass inputs was inferred from the distribution of photosynthetic activity radiation (PAR) across the year. Specific algal species were not identified in this study, organic C content was therefore derived from the average organic C content of three common wetland micro algae (Supplementary Table 2).

The areal cover of deadwood was quantified from drone imagery in January 2022, classified using the same approach as for aquatic biomass. To separate deadwood from dead reed species, the latter was manually reclassified based on the true colour orthophoto. The volume of floating deadwood in water was subsequently estimated using the *Surface Volume* tool (ArcGIS Pro 3.3.1) as the difference between water level and protruding deadwood and multiplied by two to account for submerged volume. Standing deadwood was classified separately by manual counting from orthophotos and its volume $V_{deadwood}$, estimated followingly:

$$V_{deadwood} = \int_{h_{base}}^{h_{top}} \pi r^2(h)dh\,, \tag{1}$$

where r is the radius of a tree segment, h is the length of a tree segment (4.5 m), and $h_{base} - h_{top}$ is the tree length interval between base and top. To estimate total C stored in deadwood, we used dry weight density and organic C % derived from literature values (Supplementary Table 3), wherein the northern half of wetland were attributed to the average properties of its dominant species *Quercus robur, Fraxinus excelsior*, and *Alnus glutinosa* and the southern half to the properties of *Picea abies*.

Text S3: Sediment Rock-Eval pyrolysis analysis

Following field sampling, beaver wetland sediments with permanent ($n = 13$) and intermittent inundation ($n = 13$), pre-beaver wetland sediment ($n = 8$), and forest soil ($n = 8$) samples were dried at 30 °C for 48 h and sieved with a 2 mm mesh. Samples with < 2 mm grain size were analysed with the Rock-Eval 7S analyser (Vinci Technologies, France), performing a sequential pyrolysis and oxidation to quantify hydrocarbon compounds (HC), carbon monoxide (CO) and carbon dioxide (CO_2) produced from thermal cracking of organic matter, and further partitioning organic and inorganic C following the method of Hazera et al.[1]. In the pyrolysis step, samples were heated to 200 °C to release volatile HC compounds (S1 fraction). This was followed by a temperature ramp of 25 °C min^{-1} to 650 °C, which released larger thermally cracking HC compounds derived from kerogen (S2 fraction). The S1 and S2 fractions were measured with flame ionisation detection. During pyrolysis, release of oxygen-containing compounds (S3 fraction) was measured as CO and CO_2 from organic C sources (200 – 550

°C) and CO and CO_2 from inorganic C sources (550 – 650 °C), with infrared spectroscopy. In the following oxidation step, samples were heated to 850 °C (25 °C min^{-1}), wherein organic C sources of CO and CO_2 (200 – 650 °C) were determined as the S4 fraction and inorganic CO and CO_2 (650 – 850 °C) as the S5 fraction, measured with infrared spectroscopy, respectively.

Total carbon (TC) and total organic carbon (TOC) content was calculated as the sum of total and organically derived HC, CO, and CO_2 mass. Total inorganic carbon (TIC) was determined as TC subtracted by TOC. The TOC was further partitioned into pyrolysable carbon (PC) and residual carbon (RC), operationally defined as labile organic C (PC) and recalcitrant organic C (RC), where PC = S1+S2+S3 and RC = S4+S5, excluding the inorganic fractions[2]. The organic C reactivity was further determined using the qualitative indices I and R, representing the preservation of labile organic matter (I-index) and the contribution of recalcitrant C to the total C pool (R-index)[3]. The I-index was calculated as the sum of temperature-specific integrated areas under S2 (340–400 °C), S3 (340–400 °C), and S4 (400–460 °C). The R-index was derived from the proportion of the S2 fraction integrated after 400 °C. Both I- and R-indices were calculated in the Geoworks software (Vinci Technologies).

Text S4: Sediment deposition analysis and long-term C storage

To estimate sediment deposition between the beaver dam establishment in 2010 and 2022, a spatially resolved sediment depth model (0.5 m tile size) of the wetland was generated from point measurements of sediment depths. Sediment depths were measured in March 2023 as the penetration depth of a graduated rod (n = 44) and an Edelman soil corer (n = 25). The penetration method captured the less consolidated deposits originating from post-beaver dam establishment, as the rod did not penetrate the denser, underlying pre-beaver A horizon. To interpolate the sediment depths across the entire wetland, we first generated an explanatory raster with a constant sediment depth based on the sediment depth in the lower wetland section (1.03 m). In this raster, the diminishing sediment depths towards the floodplain margins were accounted for by calculating the slope between the top of upland/levee crests and the flat section of the wetland in the lower section, using GPS measurements. The floodplain margin slopes were then used to interpolate sediment depths between top of crest (0 m depth) and the flat surface (1.03 m depth), which were subsequently applied to the entire floodplain margin boundaries of the wetland. Sediment deposition in the channel was negligible, and the channel area was therefore excluded from the analysis. To also capture the north-south sediment deposition pattern, a north-south gradient raster was created as an additional explanatory variable. Spatially distributed sediment depths were then modelled with the *Empirical Bayesian Kriging* tool (ArcGIS Pro 3.3.1), using the constant sediment depth and north-south rasters as explanatory variables, combined with sediment depth point measurements representing the dependent variable. We used a K-Bessel semivariogram model and applied log empirical transformation to prevent negative model outcomes. Finally, the sediment volume of the entire study area was calculated using the *Surface Volume* tool (ArcGIS Pro 3.3.1).

To project when the wetland would reach full sediment storage capacity, we assumed a non-linear (asymptotic) rate of change and modelled annual sediment deposition volumes (V_{sed}) for each wetland section (US, MS, and DS) with an increasing form of exponential decay accordingly:

$$V_{sed}(t) = V_{max} \cdot (1 - e^{-k(t-t_0)}) \,, \tag{2}$$

where k is the rate constant determining the non-linearity in deposition rates, t is time (year), and V_{max} is the maximum sediment volume capacity for respective section. This formulation captures the rapid initial accumulation followed by decelerating deposition as accommodation space is consumed, an approach commonly used in both natural and engineered systems where infill rates decline over time due to geometric or trapping constraints. Observed reductions in sedimentation rate with wetland age in natural beaver systems[4] and logarithmic relationships between sediment volume and wetland age[5] further support the use of this asymptotic model. V_{max} was inferred from the sum of cumulative V_{sed} estimated in 2022 and the residual sediment storage capacity (V_{res}). V_{res} was determined for each section by multiplying median wetland water volume in 2022 with the proportion of water area for each section. At the onset of beaver dam establishment (2010), sediment deposition input was set to zero. An optimal k for each section was fitted by constraining the curves to V_{max} and V_{sed} in 2022 (Supplementary Fig. 5). Complete sediment filling of the wetland was approximated as $V_{sed} > 95\%$ of V_{max} of the entire wetland. Modelled V_{sed} for 2022 was subsequently used to infer particulate organic carbon (POC) deposition in the 2022 C mass balance, assuming a POC content of 10% in fluvial sediments as they were deposited[6].

The long-term projection of C storages was based on deadwood C storage, sediment TOC (PC and RC) and TIC. Deadwood C mass was assigned as a semi-discreet input; the estimated storage in 2022 was distributed across the three years following beaver dam construction (2010-2012). After 2022, annual deadwood storage decreased at the rate of measured CO_2 emissions from dead tree stems. Annual sediment C storage was determined for each wetland section based on the V_{sed} rate, multiplied by sediment bulk density and respective sediment C contents. To separate the C storage between permanent and intermittent inundation wetland areas, sediment input into DS were equally split between permanent and intermittent pools, as the permanent inundation extent corresponded to approximately half of the DS section area. At an unknown year, we assumed that the accumulated stable C fractions of RC, TIC, and deadwood C would form the sequestered C pool of the system.

Text S5: Water balance analysis

Wetland water balance analysis

We quantified water balance dynamics in the beaver-influenced reach using paired discharge measurements at upstream (US) and downstream (DS) locations, in conjunction with estimates of wetland evapotranspiration ($ET_{wetland}$; m^3 fortnight^{-1}) and surface water storage change ($dV_{wetland}$; m^3) across the wetland area. The water balance was evaluated as:

$$\frac{dV_{wetland}}{dt} = Q_{US} - Q_{DS} - ET_{wetland} - Q_s \, , \tag{3}$$

where Q_{US} (m^3 fortnight^{-1}) is the upstream discharge, Q_{DS} (m^3 fortnight^{-1}) is the downstream discharge, Q_s (m^3 fortnight^{-1}) represents water lost to subsurface pathways (e.g., seepage or infiltration), solved as a residual term, and t is the fortnightly time step. All terms were estimated at the daily timescale and integrated to fortnightly values to reduce the noise in daily $dV_{wetland}$ estimates.

Evapotranspiration modelling and water storage change

Evapotranspiration was initially calculated in units of depth over time (ET; mm day^{-1}), using the Priestley-Taylor energy balance model[7]:

$$ET = \alpha_{PT}\left(\frac{\Delta}{\Delta + \gamma}\frac{R_n}{\lambda} - \frac{G}{\lambda}\right), \tag{4}$$

where Δ is the slope of the vapour pressure curve (kPa °C^{-1}), γ is the psychrometric constant (kPa °C^{-1}), R_n is the net surface radiation (MJ m^{-2} day^{-1}), λ is the latent heat of vaporisation (MJ kg^{-1}), G is the heat flux into the water column/sediment (MJ m^{-2} day^{-1}) and α_{PT} is the Priestley-Taylor coefficient. The α_{PT} coefficient represents the effect of warm and dry air exchange near the water surface[8], where values of $\alpha_{PT} > 1$ denote an increase in vapour pressure deficit, enabled by higher surface resistance. We used $\alpha_{PT} = 1$, reflecting humid, open-canopy conditions.

To resolve the $ET_{wetland}$ term, acting on the inundated surface, and determine $dV_{wetland}$, we estimated daily water surface area and volume using drone-based RGB imagery collected during six surveys in 2022. Water extent for each survey was mapped with supervised classification, using ArcGIS Pro (3.3.1) toolboxes *Train Support Vector Machine Classifier* and *Classify Raster*. Then, water extent at daily resolution across up-, mid-, and downstream wetland sections were estimated from relationships between water stage (at DS) and observed water surface area, fitted using linear or logarithmic regressions (Supplementary Fig. 7). To avoid water surface overestimation, linear relationships were fitted for the observed range of water surface area. Above this range, another linear regression was fitted between the maximum observed water surface area and total surface area. For the upstream wetland section, daily water surface area was fitted with a logarithmic function as this section only showed limited inundation throughout 2022.

To determine $dV_{wetland}$, total water volume (channel and wetland) was calculated for each of the six occasions with identified water extents. Water volume was interpolated with the ArcGIS Pro (3.3.1) toolbox *Surface volume*, using the relative elevation difference between measured wetland stage and a 0.5 m resolution DEM[9]. Determined water volume in the entire study area was validated by its correlation to total water surface area ($R^2 = 0.94$, $p < 0.01$). Subsequently, daily water volume was estimated by fitting a logarithmic relationship between water volume and respective water stage at DS location (Supplementary Fig. 8). The DS location was chosen since it resulted in the best fit to water volumes.

Text S6: Load estimation and dissolved carbon partitioning

The processing of dissolved C loads was partitioned into biological assimilation and production, wetland storage changes, and subsurface storage/losses. For DOC loads, the assimilation pathway was excluded. The partitioning was performed on the fortnightly sum of DIC and DOC loads. Biological assimilation and production of dissolved C loads (dC_{bio}) were inferred from concentration changes, representing mass removal not attributed to passive hydrological removal:

$$dC_{bio} = \frac{(C_{conc\_US} - C_{conc\_DS}) \times Q_{US}}{1000}, \tag{5}$$

where C_{conc_US} and C_{conc_DS} are the dissolved C concentrations at upstream and downstream locations respectively, and 1000 is a unit conversion factor. Subsequently, dC_{bio} was partitioned into DIC assimilation ($dC_{bio} > 0$) and DIC, DOC production ($dC_{bio} < 0$). To infer the dissolved C loads stored or released from wetland surface water, we first determined the changes in dissolved C loads removed via hydrological processes ($dC_{hydrology}$; Equation 6) and the surface water storage fraction ($dV_{fraction}$ [-]; Equation 7):

$$dC_{hydrology} = dC_{tot} - dC_{bio}\ , \tag{6}$$

$$dV_{fraction} = \frac{dV_{wetland}}{dt} \Big/ \left(\frac{dV_{wetland}}{dt} + Q_s\right), \tag{7}$$

where dC_{tot} is the total change in dissolved C loads and t is the fortnightly time step. We finally derived dissolved C loads removed or released from the wetland storage (dC_V) and removed via subsurface storage and infiltration (dC_{Q_s}) followingly:

$$dC_V = dC_{hydrology} \times dV_{fraction} \tag{8}$$

$$dC_{Q\_s} = dC_{hydrology} - dC_V \tag{9}$$

Text S7: Stream corridor counterfactual scenario

To support the revised C balance of the forested counterfactual scenario, shown in Table S1, we assumed a net primary production (NPP) of 7.0 t C ha^{-1} yr^{-1}, based on reported values for mixed oak-hornbeam forests (*Quercus robur, Carpinus betulus, Fraxinus excelsior*) on moderately dry soils such as those of the Marthalen region. This NPP estimate is admittedly subjective but falls within the range reported for productive temperate deciduous systems[10,11], and is slightly higher than the 5.3 t C ha^{-1} yr^{-1} observed at the nearby Neunkirch site, which is dominated by *Fagus sylvatica* and exhibits lower productivity due to its closed canopy and species-specific traits[12].

To estimate heterotrophic soil respiration (R_{h_soil}), not accounted for in the NPP value, static chamber CO_2 evasion measurements of forest soils (11.2 t C ha^{-1} yr^{-1}) was partitioned into R_{h_soil} (6.7 t C ha^{-1} yr^{-1}) and autotrophic root respiration (R_{a_root}; 4.5 t C ha^{-1} yr^{-1}), assuming a R_{a_root}/R_{h_soil} ratio = 0.66 consistent with values reported in forest soils[13]. To capture total R_a, we added estimates of aboveground maintenance and growth respiration (R_{a_above}) to our R_{a_root} estimate, yielding a total R_a = 6.2 t C ha^{-1} yr^{-1}. This places R_a at ~42% of gross primary production (GPP), and results in GPP = 13.2 t C ha^{-1} yr^{-1}, aligning with forest flux tower data across temperate Europe and returning an NPP/GPP ratio close to the expected range (carbon use effectiveness ≈ 0.58).

The stream was assumed to be net heterotrophic, as aquatic CO_2 evasion from the 0.36 ha stream reach was measured at 10.2 t C ha^{-1} yr^{-1}, greatly exceeding our added aquatic GPP estimate of 1 t C ha^{-1} yr^{-1}, observed in shaded temperate streams[14]. When combining all terrestrial and aquatic inputs (26.0 t C yr^{-1}) with outputs (25.5 t C yr^{-1}), the resulting net C balance is 0.5 t C yr^{-1} across the full reach. Projected over a 33-year period, equivalent to the modelled lifespan of the beaver-impacted wetland, the forested counterfactual represents a long-term C sink of 16.5 t C. These values are internally consistent and offer a conservative yet ecologically robust scenario for assessing the biogeochemical consequences of beaver-driven floodplain rewetting.

While this counterfactual scenario provides a traceable and physiologically consistent estimate, its long-term C balance is sensitive to two key components: aquatic CO_2 emissions and forest NPP. If aquatic CO_2 evasion were overestimated, e.g., due to chamber bias, limited diel coverage, or higher floodplain inundation under forested conditions, then lowering the flux by 25% would reduce annual aquatic efflux from 4.1 to ~3.1 t C yr^{-1}, increasing the net C balance to ~1.5 t C yr^{-1}. Conversely, if aquatic CO_2 losses are underestimated, e.g., due to nighttime degassing or wind-driven turbulence, total evasion could plausibly rise to 12 – 13 t C ha^{-1} yr^{-1}, resulting in annual aquatic efflux of ~4.8 – 5.2 t C yr^{-1}, and reducing the net C balance accordingly. Similarly, if forest NPP were closer to the 5.3 t C ha^{-1} yr^{-1} measured at the nearby Neunkirch flux site, rather than the 7.0 t C ha^{-1} yr^{-1} used here, then NEP would decline from 0.5 t C ha^{-1} yr^{-1} to below zero, rendering the forest C neutral or even a weak source when aquatic CO_2 evasion is included. Combining the lower-bound NPP with the upperbound aquatic efflux would reduce the long-term net C sink to close to zero, whereas higher NPP and lower aquatic CO_2 evasion would yield a cumulative sink of ~50 t C over 33 years. These bounds underscore that while the best-estimate scenario suggests a modest net C sink, the true C balance of the counterfactual scenario likely ranges from weak source to moderate sink, depending on ecosystem productivity and aquatic exchange dynamics.

Text S8: National upscaling of C sequestration

To estimate the potential C sequestration benefits of beaver-driven floodplain restoration at the national scale, we scaled the measured sediment C burial rate from the Marthalen wetland (4.71 t C ha^{-1} yr^{-1}) to mapped lowland floodplain areas in Switzerland identified as suitable for beaver recolonisation[15]. Using national floodplain assessments, we considered two area scenarios: (i) the 300 km^2 of "opportunity" zones, where restoration is ecologically and logistically feasible, and (ii) the broader 450 km^2 encompassing both "opportunity" and "conflict" zones, where floodplain function could potentially be restored under more enabling policy or management conditions. However, this also presupposes efforts to minimise emergent land use conflicts (e.g., agricultural activities and drinking water treatment).

Applying the field-based burial rate to these areas yields an estimated annual C burial of ~141,200 t C yr^{-1} across opportunity zones, and ~211,700 t C yr^{-1} if the full area including conflict zones were reactivated. These values reflect only long-term sediment C burial, excluding deadwood and transient biomass pools, and assume full functional saturation by beaver activity. While optimistic in spatial extent, the burial rate itself is conservative in that it excludes potential C benefits from avoided decomposition or methane offsets.

Supplementary Figures

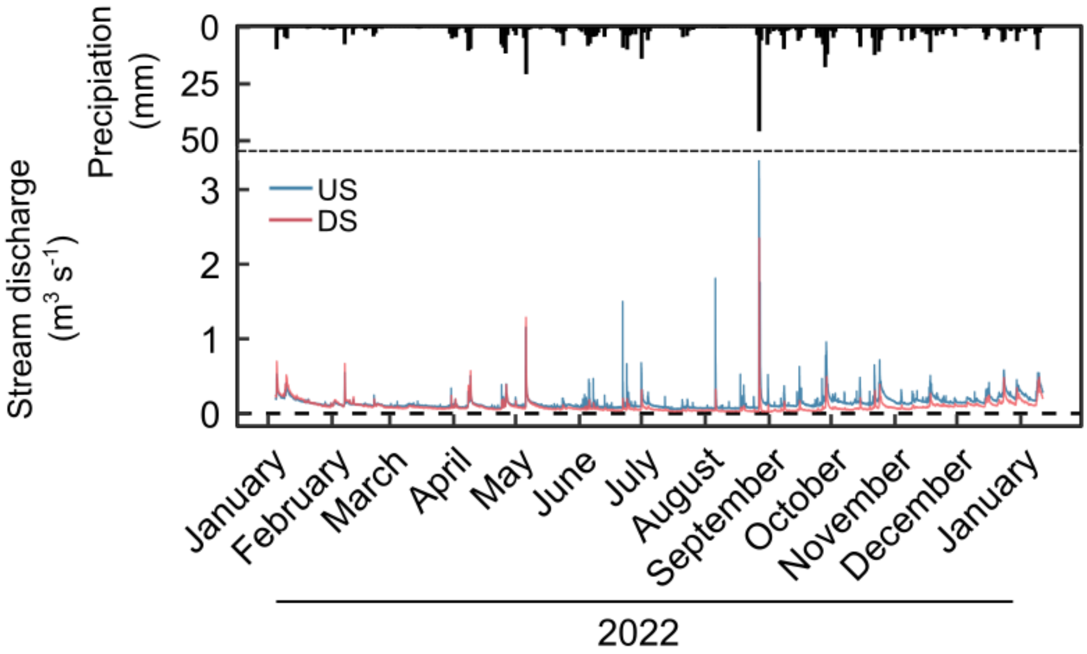

Fig. S1. Precipitation from a nearby weather station and stream discharge at upstream (US) and downstream (DS) monitoring locations.

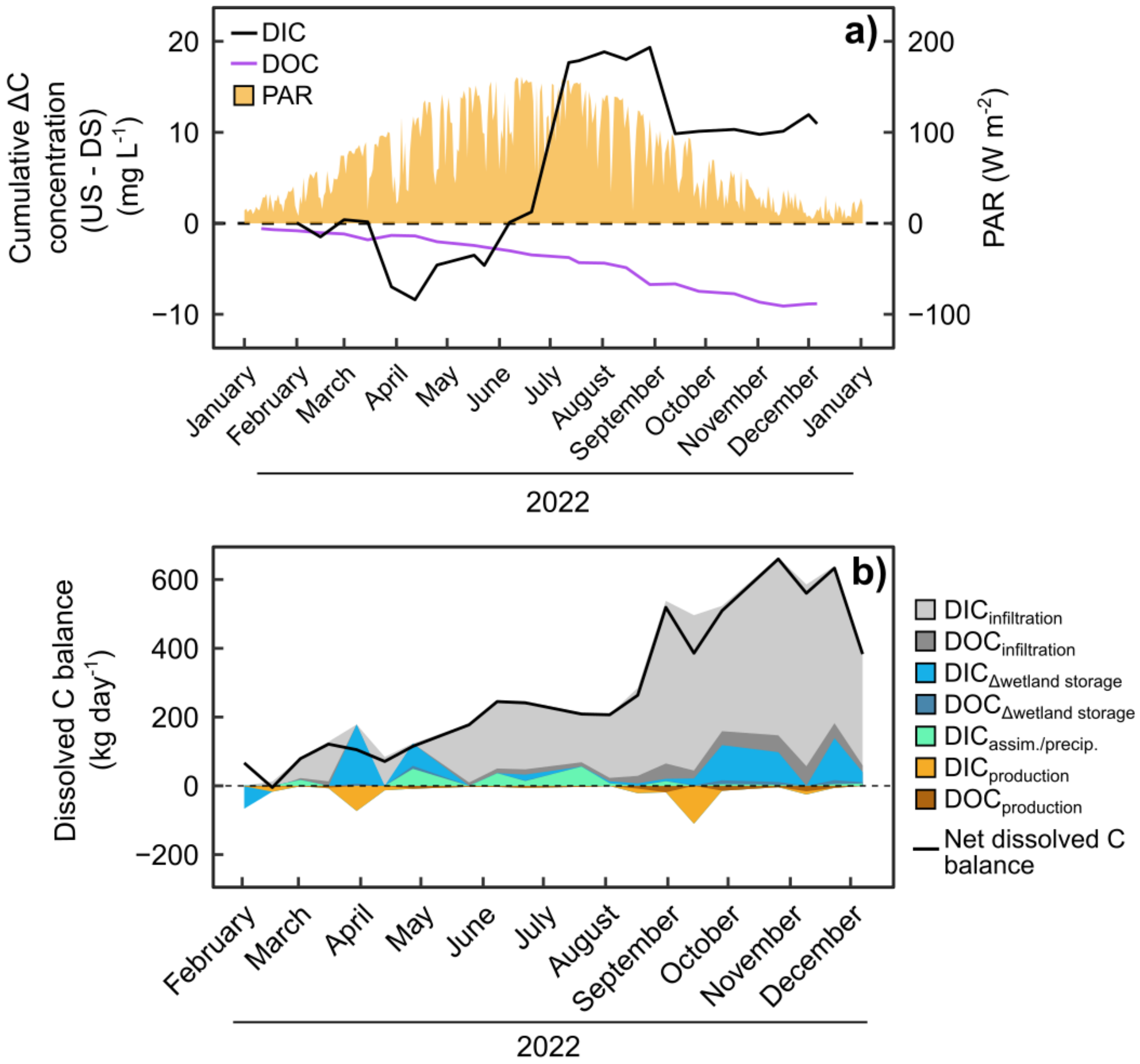

Fig. S2. a) Time series of cumulative changes in dissolved inorganic carbon (DIC) and dissolved organic carbon (DOC) concentrations between upstream (US) and downstream (DS) locations, compared to photosynthetically active radiation (PAR). Positive concentration values (left axis) indicate downstream reduction in concentrations. **b)** Annual mass balance of DIC and DOC loads, partitioned by infiltration, changes in wetland storage change (Δwetland storage subscript), assimilation and precipitation of DIC (assim./precip. subscript), and biogeochemical production (production subscript), estimated at fortnightly intervals.

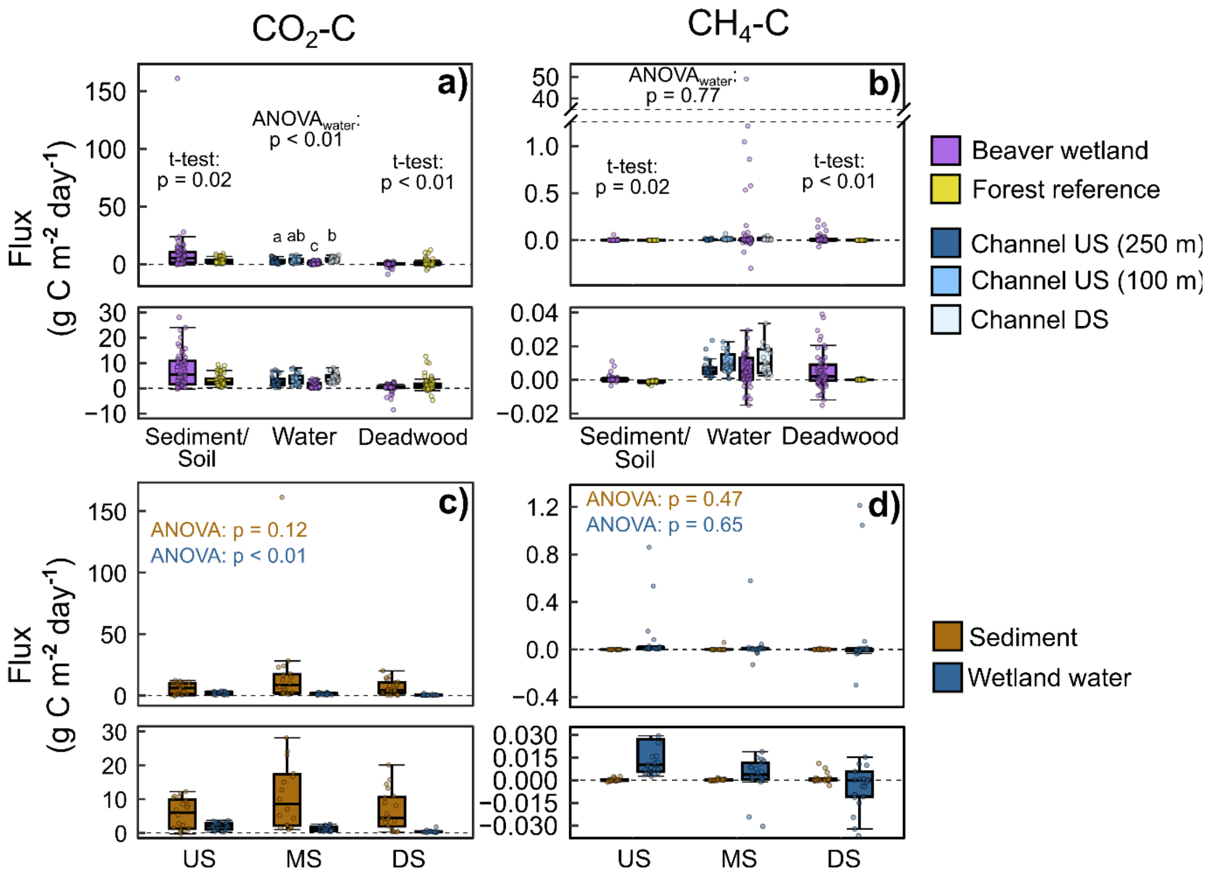

Fig. S3. a, b) Fluxes of CO_2-C and CH_4-C from beaver wetland interfaces (exposed sediments, wetland water, and deadwood), channel water, and nearby forest reference soils and deadwood. **c, d)** Spatial distribution of CO_2-C and CH_4-C fluxes in exposed sediments and wetland water across the wetland sections. P-values of t-tests and ANOVA tests, including post-hoc Tukey tests are shown within panels.

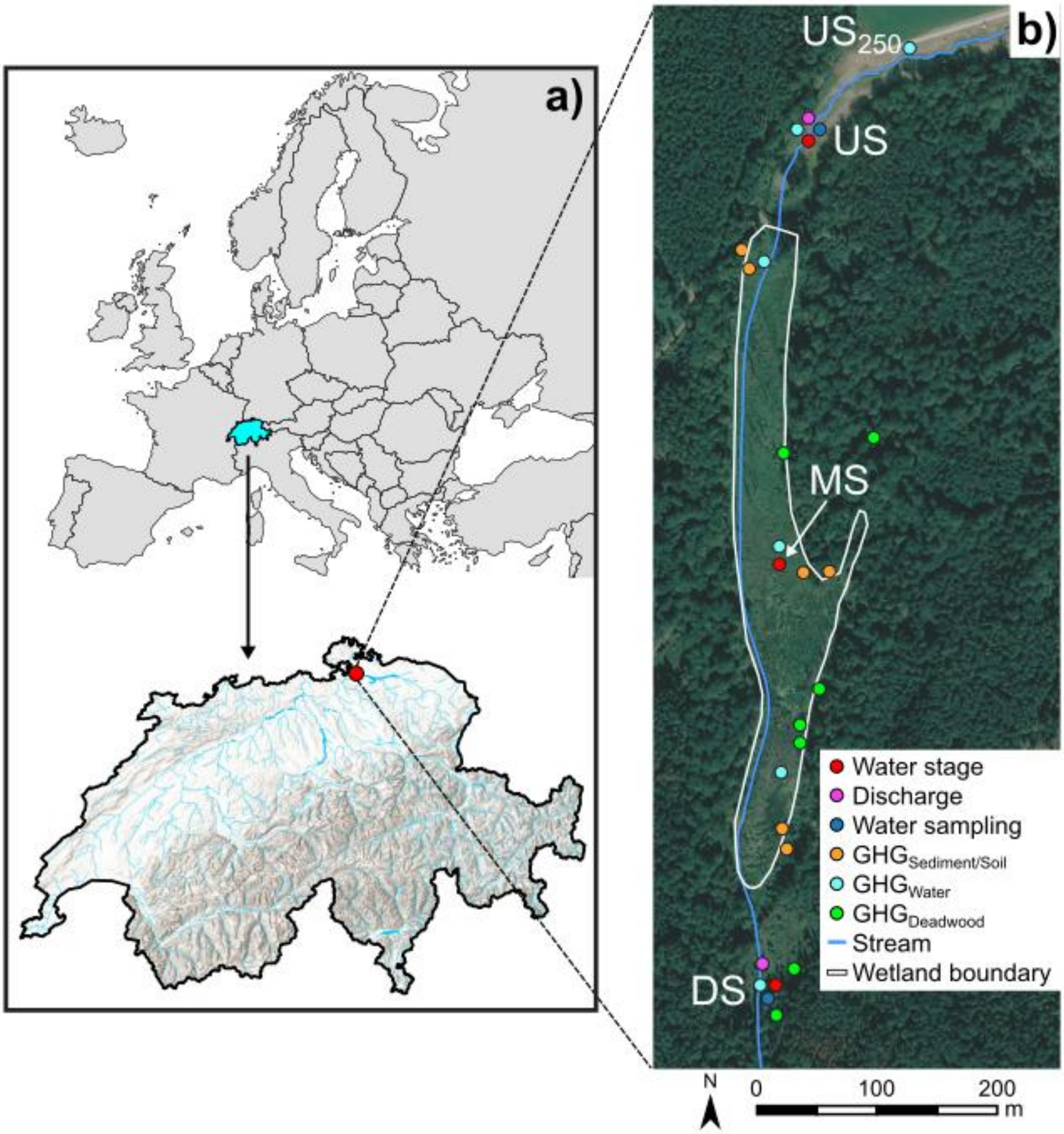

Fig. S4. **a)** Location of study area in northern Switzerland. **b)** Satellite image of the study area, showing monitoring and sampling locations and delineated beaver wetland area. US = upstream, US_{250} = upstream, 250 m from wetland, MS = midstream, DS = downstream. Satellite image: Google, ©2024 CNES/Airbus.

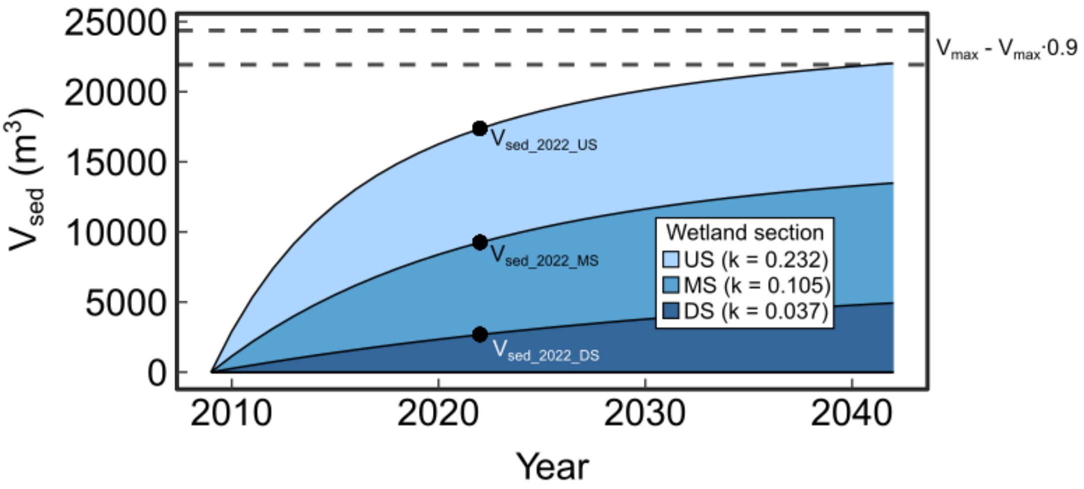

Fig. S5. Non-linear fitting of annual sediment deposition volume (V_{sed}) for upstream (US), midstream (MS), and downstream (DS) wetland sections. The optimal rate constant (k) was identified for the curve intersecting estimated sediment deposition in 2022 (V_{sed_2022}). Complete sediment filling of the wetland was approximated as V_{sed} > 90% of maximum sediment volume capacity (V_{max}) of the entire wetland.

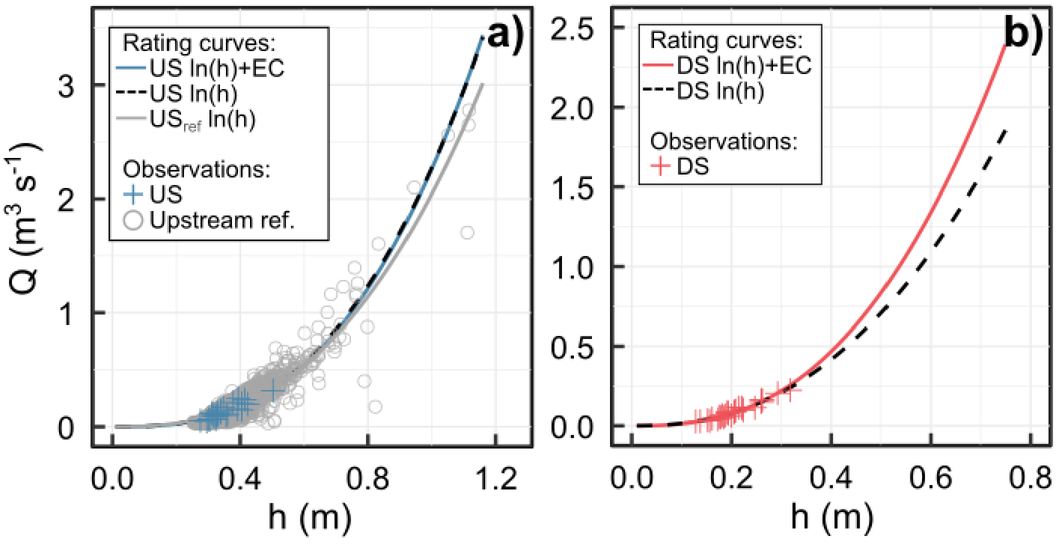

US			DS		
Model	**R^2**	**AIC**	**Model**	**R^2**	**AIC**
ln(h)+EC	0.78	-0.86	ln(h)+EC	0.94	-27.49
ln(h)	0.75	2.63	ln(h)	0.94	-29.37

Fig. S6. Discharge (Q) rating curves and observed Q at **a)** upstream (US), upstream reference, and **b)** downstream (DS) locations. h = water stage and EC = electrical conductivity. The table show goodness-of-fit for the two models ln(Q) = ln(h) and ln(Q) = ln(h) + EC, including coefficient of determination (R^2) determined from leave-one-out cross validation, and Akaike's information criterion (AIC).

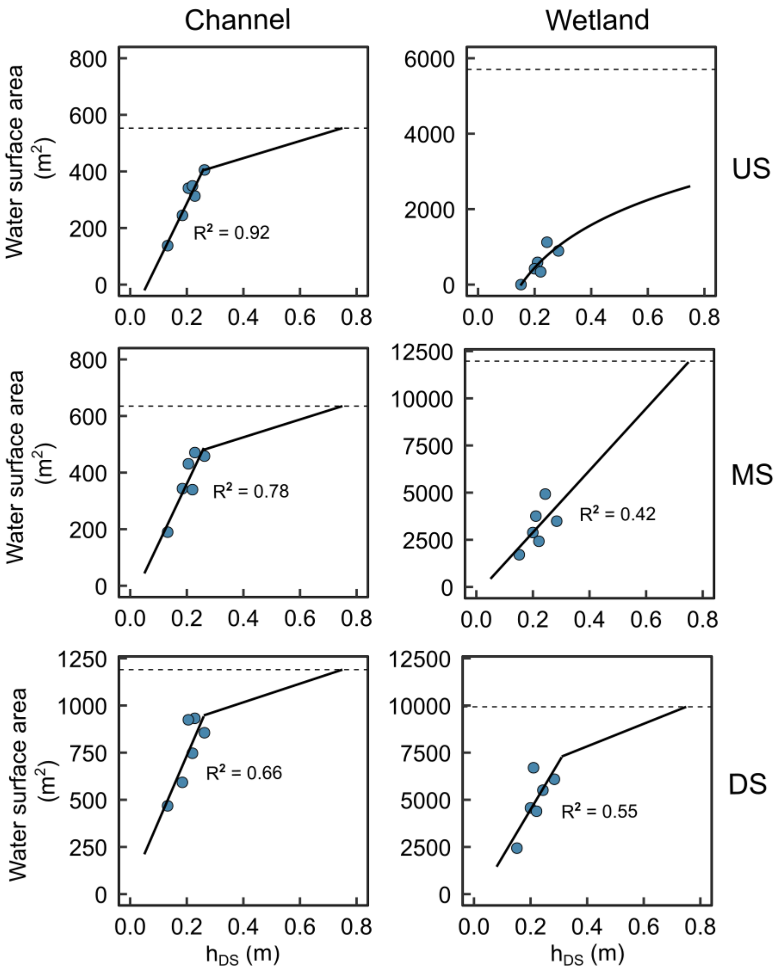

Fig. S7. Relationship between water surface area and water stage at downstream location (h_{DS}) in upstream (US), midstream (MS) and downstream (DS) sections of the beaver wetland. Dashed lines show the total surface area in respective sections. Coefficient of determination (R^2) is shown for linear regressions.

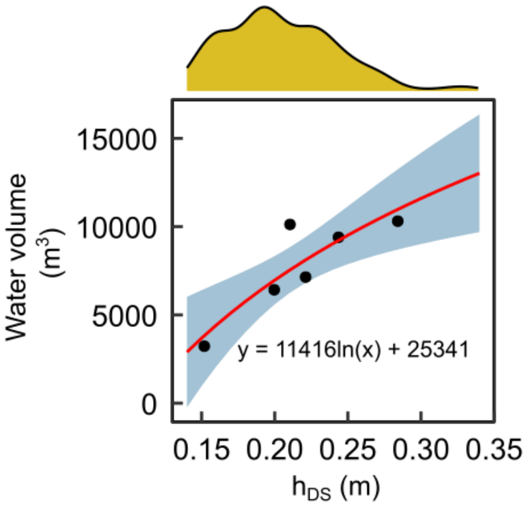

Fig. S8. Relationship between total water volume (channel and wetland) and water stage at downstream location (h_{DS}), averaged by week. The density distribution of water stages is shown above the panel in yellow.

Supplementary Tables

Table S1. Terrestrial C balance and total ecosystem inputs and outputs for counterfactual scenario of the studied reach without beaver activity. NPP_{ter} = terrestrial net primary production, R_{h_soil} = heterotrophic soil respiration, R_{a_root} = autotrophic root respiration, R_{a_above} = autotrophic aboveground respiration, GPP_{ter} = terrestrial gross primary production, NEP_{ter} = terrestrial net ecosystem production, GPP_{aq} = aquatic gross primary production.

Component	Area (ha)	Flux (t C ha^{-1} yr^{-1})	Total (t C yr^{-1})	Notes / assumptions
Terrestrial C balance				
NPP_{ter}	3.2	7	22.4	Oak-hornbeam productivity (see Text S7)
R_{h_soil}	3.2	6.7	21.4	R_{h_soil} + R_{a_root} = measured soil CO_2 flux *and* R_{a_soil} / R_{h_root} = 0.66
R_{a_root}	3.2	4.5	14.4	R_{h_soil} + R_{a_root} = measured soil CO_2 flux *and* R_{a_soil} / R_{h_root} = 0.66
R_{a_above}	3.2	1.7	5.4	GPP = NPP + R_{a_root} + R_{a_above} *and* (R_{a_root} + R_{a_above}) / GPP_{ter} = 0.42
GPP_{ter}	3.2	13.2	42.2	GPP = NPP + R_{a_root} + R_{a_above} *and* (R_{a_root} + R_{a_above}) / GPP_{ter} = 0.42
NEP_{ter}	3.2	0.3	1.0	NEP_{ter} = NPP_{ter} - R_{h_soil}
Inputs				
NPP_{ter}	3.2	7	22.4	
Coarse woody debris input	3.2	1	3.2	Assumed coarse woody debris for temperate forest
GPP_{aq}	0.4	1	0.4	Assumed aquatic GPP of shaded streams (see Text S7)
Total inputs	**-**	**-**	**26.0**	
Outputs				
R_{h_soil}	3.2	6.7	21.4	
Aquatic CO_2 evasion	0.4	10.2	4.1	Chamber-based measurement
Total outputs	**-**	**-**	**25.5**	
Net ecosystem balance	**3.6**	**0.1**	**0.5**	Total inputs – total outputs
Long-term projection (33 years)	**3.6**	**3.3**	**16.5**	Projected net C accumulation

Table S2. Macrophyte and algal biomass, carbon content, surface cover and total organic carbon (OC) input of the identified species in the beaver wetland (mean ± one standard deviation). References indicate values derived from literature.

Species	**Biomass (g DW m^{-2})**	**OC% in biomass (DW)**	**Surface cover (m^{2})**	**OC input (t yr^{-1})**
Phalaris arundinacea	1,586.90	45.00 ± 0.59[16]	16,818.17	12.01 ± 0.16
Stachys palustris	2,200.00	44.40 ± 0.84[17*]	5,178.95	5.06 ± 0.10
Nasturtium officinale	2,406.25	44.77 ± 0.02[18]	2,305.10	2.48 ± 0.00
Sparganium erectum.	140.00	44.79 ± 0.53[19]	3,038.41	0.19 ± 0.00
Ceratophyllum demersum	958.10	39.37 ± 3.94[20]	1,958.58	0.74 ± 0.07
Micro algae *(Chlorella vulgaris, Chlamydomonas Reinhardtii, Spirulina platensis)*	139.40	47.03 ± 4.22[21]	897.91	0.06 ± 0.00
Total annual OC input from aquatic vegetation				20.54 ± 0.20

[*] *Stachys palustris* C content is based on the global average in herbaceous vegetation from Ma et al.[17]

Table S3. Deadwood biomass, carbon content, surface cover and total organic carbon (OC) storage of the deposited deadwood in the beaver wetland (mean ± one standard deviation). References indicate values derived from literature.

Species	**Biomass (g DW m^{-2})**	**OC% in biomass (DW)**	**Volume (m^{3})**	**OC storage (t yr^{-1})**
Picea abies	356 ± 1.7[22]	50.30 ± 0.1[23]	1425.3	255.2 ± 1.2
Quercus robur	584.3 ± 1.53[24]	49.02 ± 0.50[25]	292.8	83.9 ± 0.2
Fraxinus excelsior	606 ± 38[26]	49.29 ± 0.08[25]	292.8	87.5 ± 5.5
Alnus glutinosa	499.75 ± 50[27]	50.47 ± 0.39[25]	292.8	73.8 ± 7.4
Total annual OC storage in deadwood				500.4 ± 9.3

Table S4. Goodness-of-fit parameters for daily loads of dissolved inorganic carbon (DIC), dissolved organic carbon (DOC), and suspended sediments (SS), modelled with WRTDS. Subscripts denote the monitoring locations upstream (US) and downstream (DS). RMSE = root mean squared error, R^2 = coefficient of determination, SE = standard error of the estimate, and NSE = Nash-Sutcliffe efficiency.

Parameters	**RMSE (ln units)**	**R^2 ln(concentration)**	**R^2 ln(load)**	**SE (%)**
DIC$_{\mathrm{US}}$	0.15	0.06	0.85	14.9
DIC$_{\mathrm{DS}}$	0.12	0.43	0.95	12.2
DOC$_{\mathrm{US}}$	0.28	-0.19	0.73	28.3
DOC$_{\mathrm{DS}}$	0.25	0.08	0.87	24.8
SS$_{\mathrm{US}}$	0.88	0.49	0.56	107.0
SS$_{\mathrm{DS}}$	0.94	0.42	0.65	118.0

Table S5. Multiple linear regression explaining the variability of CO_2-C fluxes from exposed sediment in 2022, by each wetland section (up-, mid-, and downstream). Air temperature (°C) and exposed surface area (m^2) were used as predictors.

Predictors	**Scaled β coefficient**	**p-value**
Upstream section		
Air temperature	4.88	< 0.01
Exposed surface area	0.26	0.80
Midstream section		
Air temperature	4.61	< 0.01
Exposed surface area	1.39	0.19
Downstream section		
Air temperature	4.09	< 0.01
Exposed surface area	0.559	0.58

References

1. Hazera, J. *et al.* Adjustments to the Rock-Eval thermal analysis for soil organic and inorganic carbon quantification. *Biogeosciences* **20**, 5229–5242 (2023).
2. Carrie, J., Sanei, H. & Stern, G. Standardisation of Rock–Eval pyrolysis for the analysis of recent sediments and soils. *Org. Geochem.* **46**, 38–53 (2012).
3. Sebag, D. *et al.* Dynamics of soil organic matter based on new Rock-Eval indices. *Geoderma* **284**, 185–203 (2016).
4. Meentemeyer, R. K. & Butler, D. R. Hydrogeomorphic Effects of Beaver Dams in Glacier National Park, Montana. *Phys. Geogr.* **20**, 436–446 (1999).
5. Dunn, S. B., Rathburn, S. L. & Wohl, E. Post-fire sediment attenuation in beaver ponds, Rocky Mountains, CO and WY, USA. *Earth Surf. Process. Landf.* **49**, 4340–4354 (2024).
6. Hoffmann, T. O., Baulig, Y., Fischer, H. & Blöthe, J. Scale breaks of suspended sediment rating in large rivers in Germany induced by organic matter. *Earth Surf. Dyn.* **8**, 661–678 (2020).
7. Priestley, C. H. B. & Taylor, R. J. On the Assessment of Surface Heat Flux and Evaporation Using Large-Scale Parameters. *Mon. Weather Rev.* **100**, 81–92. (1972).
8. McMahon, T. A., Peel, M. C., Lowe, L., Srikanthan, R. & McVicar, T. R. Estimating actual, potential, reference crop and pan evaporation using standard meteorological data: a pragmatic synthesis. *Hydrol. Earth Syst. Sci.* **17**, 1331–1363 (2013).
9. Swisstopo. swissALTI3D. https://www.swisstopo.admin.ch/en/height-model-swissalti3d#swissALTI3D---Download (2019**)**.
10. Pretzsch, H. Forest Dynamics, Growth, and Yield. in *Forest Dynamics, Growth and Yield: From Measurement to Model* (ed. Pretzsch, H.) 1–39 (Springer, Berlin, Heidelberg, 2009). doi:10.1007/978-3-540-88307-4_1
11. Luyssaert, S. *et al.* Old-growth forests as global carbon sinks. *Nature* **455**, 213–215 (2008).
12. Etzold, S., Waldner, P., Thimonier, A., Schmitt, M. & Dobbertin, M. Tree growth in Swiss forests between 1995 and 2010 in relation to climate and stand conditions: Recent disturbances matter. *For. Ecol. Manage.* **311**, 41–55 (2014).

13. Jin, Z. *et al.* A global surface CO_2 flux dataset (2015–2022) inferred from OCO-2 retrievals using the GONGGA inversion system. *Earth Syst. Sci. Data* **16**, 2857–2876 (2024).

14. Bernhardt, E. S. *et al.* Light and flow regimes regulate the metabolism of rivers. *Proc. Natl. Acad. Sci. U.S.A.* **119**, e2121976119 (2022).

15. Dennis, M., Angst, C., Larsen, J. R., Rey, E. & Larsen, A. A national scale floodplain model revealing channel gradient as a key determinant of beaver dam occurrence and inundation potential can anticipate land-use based opportunities and conflicts for river restoration. *Glob. Ecol. Conserv.* **56**, e03304 (2024).

16. Ge, Z.-M. *et al.* Carbon assimilation and allocation (13C labeling) in a boreal perennial grass (*Phalaris arundinacea*) subjected to elevated temperature and CO2 through a growing season. *Environ. Exp. Bot.* **75**, 150–158 (2012).

17. Ma, S. *et al.* Variations and determinants of carbon content in plants: a global synthesis. *Biogeosciences* **15**, 693–702 (2018).

18. Maqbool, C. & Khan, A. B. Biomass and Carbon Content of Emergent Macrophytes in Lake Manasbal, Kashmir: Implications for Carbon Capture and Sequestration. *Int. J. Sci. Res.* **3**, (2013).

19. Kulikova, Y. *et al.* Analysis of Resource Potential of Emergent Aquatic Vegetation in the Curonian Lagoon of the Baltic Sea. *Water* **15**, 2136 (2023).

20. Kusolsongtawee, T., Wuttilerts, T., Chulalaksananukul, S. & Maneechot, L. Bioethanol Production from Ceratophyllum demersum L. and Carbon Footprint Evaluation. *Appl. Sci. Eng. Prog.* **11**, 103-108 (2018).

21. Halder, P. & Azad, A. K. Chapter 7 - Recent trends and challenges of algal biofuel conversion technologies. in *Advanced Biofuels* (eds. Azad, A. K. & Rasul, M.) 167–179 (Woodhead Publishing, 2019). doi:10.1016/B978-0-08-102791-2.00007-6.

22. Sopushynskyy, I., Kharyton, I., Teischinger, A., Mayevskyy, V. & Hrynyk, H. Wood density and annual growth variability of Picea abies (L.) Karst. growing in the Ukrainian Carpathians. *Eur. J. Wood Prod.* **75**, 419–428 (2017).

23. Jagodziński, A. M., Dyderski, M. K. & Horodecki, P. Differences in biomass production and carbon sequestration between highland and lowland stands of *Picea abies* (L.) H. Karst. and *Fagus sylvatica* L. *For. Ecol. Manage.* **474**, 118329 (2020).

24. Vavrčík, H. & Gryc, V. Analysis of the annual ring structure and wood density relations in English oak and Sessile oak. *Wood Res.* **57**, (2012).

25. Matthews, G. *The Carbon Content of Trees*. (Forestry Commission, 1993).

26. Le Goff, N., Granier, A., Ottorini, J.-M. & Peiffer, M. Biomass increment and carbon balance of ash (Fraxinus excelsior) trees in an experimental stand in northeastern France. *Ann. For. Sci.* **61**, 577–588 (2004).

27. Meier, E. European alder | The Wood Database (Hardwood). https://www.wood-database.com/european-alder/ (2010).